Nano Energy 49 (2018) 257–266

Contents lists available at ScienceDirect

Nano Energy

journal homepage: www.elsevier.com/locate/nanoen

Full paper

Effective atomic interface engineering in $Bi_2Te_{2.7}Se_{0.3}$ thermoelectric material by atomic-layer-deposition approach

Shuankui Li[a], Yidong Liu[a], Fusheng Liu[b], Dongsheng He[c], Jiaqing He[c], Jun Luo[d], Yinguo Xiao[a], Feng Pan[a,*]

[a] School of Advanced Materials, Peking University Shenzhen Graduate School, Shenzhen 518055, China
[b] College of Materials Science and Engineering, Shenzhen University and Shenzhen Key Laboratory of Special Functional Materials, Shenzhen 518060, China
[c] Department of Physics, South University of Science and Technology of China, Shenzhen 518055, China
[d] School of Materials Science and Engineering, Shanghai University, Shanghai 200444, China

ARTICLE INFO

Keywords:
Thermoelectric
Bi_2Te_3
Atomic-Layer-Deposition
Nanocomposites
Energy filtering

ABSTRACT

Grain boundaries play a critical role in the carrier/phonon transport in thermoelectric materials. It remains a big challenge to control over both chemical composition and dimension of grain boundary precisely by traditional approaches. Herein, an bottom-up grain boundary engineering strategy based on atomic layer deposition (ALD) is first introduced to atomically control and modify the grain boundary of Bi_2Te_3-based thermoelectric materials. To demonstrate the effect of this strategy, ultrathin ZnO interlayer is deposited on the $Bi_2Te_{2.7}Se_{0.3}$ (BTS) grain boundaries to optimize of the carrier/phonon transport for achieving high thermoelectric performance. In situ TEM experiments upon heating reveals that the ZnO interlayer will give rise to the precipitation of Te nanodot at ZnO/BTS interface, which can be atomically controlled by adjusting the thickness of ZnO layer. Benefited from the atomically precise modified grain boundary, a maximum ZT of 0.85 is obtained, approximately 1.8 times higher than that of the pure BTS. As a powerful interfacial modification strategy, ALD-based approach can be extended to other thermoelectric material system simply, which may contribute to the development of high performance thermoelectric material of great significance.

1. Introduction

Thermoelectric (TE) materials allowing direct conversion of heat into electricity have drawn worldwide interests for decades due to their potential application in energy harvesting from wasted heat sources. [1,2] To maximize the energy conversion efficiency by turning the electron and phonon transport properties is an essential issue in research of thermoelectric materials. [3] Controlling and modifying of the grain or phase boundaries of thermoelectric materials to partially decouple electrical conductivity (σ) and Seebeck coefficient (S) and thermal conductivity (κ) is an basic principle on the development of high performance thermoelectric material. [4] Previous investigations about controlling boundaries primarily focused on the reducing grain size or introducing nanoinclusions, such as $Bi_2Te_{2.7}S_{0.3}/Bi_2Te_3$ heteronanosheet, [5] Au nanodot/ Bi_2Te_3 nanotube, [6] and $Bi_2Te_{2.7}S_{0.3}/SnS_2$ nanocomposites. [7] In such conventional thermoelectric materials, the grain or phase boundaries is expected to suppress lattice thermal conductivity (phonon scattering) while raise Seebeck coefficient through energy filtering effect. However, such energy filtering effect at grain or phase boundaries could always lead to the reduction of carrier mobility, which will hamper the improvement of power factor (PF = $S^2\sigma$). [8–10] The grain boundary engineering in thermoelectric materials has been considered as an effective way to solve the above problems, since it can enhance S without hurting σ much, resulting in a net enhancement in $S^2\sigma$ as theoretically predicted. [14–17] Unfortunately, there are only few experimental reports to meet this challenge because it is difficult to control both the chemical composition and the dimension of boundaries by the traditional approach.

Atomic layer deposition (ALD) is a promising approach to meet the above challenges. In contrast to the traditional interface modification method, bottom-up grain boundary engineering in thermoelectric materials can be effectively realized at atomic-level, which may contribute to the development of high performance thermoelectric material of great significance. ALD employs saturated, self-limiting surface-chemistry reactions and allows for thin-film materials to grow one layer at a time, so that, any complex three-dimensional (3D) structures can be conformally and uniformly coated by ALD with atomically precise control over film composition and thickness. These prominent features

* Corresponding author.
E-mail address: panfeng@pkusz.edu.cn (F. Pan).

https://doi.org/10.1016/j.nanoen.2018.04.047
Received 14 February 2018; Received in revised form 2 April 2018; Accepted 16 April 2018
Available online 17 April 2018
2211-2855/ © 2018 Elsevier Ltd. All rights reserved.

make ALD particularly useful for improving the thermoelectric performance by engineering the grain boundary of thermoelectric materials, given that the grain boundaries play a critical role in the carrier/phonon transport. On the other hand, as a bottom-up grain boundary engineering strategy, ALD allows for designing the grain boundaries with particular component and special function. [18–21] The motivation of this work is to explore an ALD based general approach in designing and controlling of the grain boundary of TE materials, which will finally contribute to the development of high performance TE materials.

Taking into account the advantages of ALD, we herein propose a ALD-based general bottom-up strategy to design and control grain boundary and investigate the relationship between grain boundary and the electron/phonon transportation behavior in n-type $Bi_2Te_{2.7}Se_{0.3}$ (BTS) TE materials. As a wide band-gap semiconductor with tunable electrical conductivity, a n-type Zinc oxide (ZnO) layer is introduced at the BTS grain boundary to investigate the interface-related carrier/phonon transport. [22] In situ TEM experiments upon heating reveals that the ZnO layers could give rise to the precipitation of Te nanodot at ZnO/BTS interface, which could be accurately controlled in atomic scale by adjusting the thickness of ZnO layers. With optimized thickness of ZnO layers (~ 2 nm, 20cycles), sawtooth ZnO/BTS boundary with atomic scale undulation formed, which lead to strong enhancement in S ($-261\mu V/K$) and $S^2\sigma$ ($\sim 25.1\mu W/cmK^2$) due to energy filtering effects. Thus, by introducing the ultrathin ZnO interlayer on the grain boundary of BTS, the potential barrier and grain size are optimized to satisfy the relationship $\lambda_p < d < \lambda_e$, thereby, the greatly improved S is obtained without hurting σ much, which results in a net improvement in $S^2\sigma$. Simultaneously, the ZnO/BTS interface could suppress the bipolar thermal conductivity at high temperature region. As a result, the optimization and regulation of the electron and phonon transport properties has achieved, the ZT display an over 80% enhancement compared with pure BTS. These results demonstrate that ALD-based approach is a facile, scalable and low-energy-intensive way to achieve atomic scale grain boundary regulation, which can open up great possibilities in developing high-performance thermoelectric material.

2. Experimental section

2.1. Materials

TeO_2 powder (99.999%), SeO_2 powder (99.999%), $Bi(NO_3)_3{\cdot}5H_2O$ (99.999%), NaOH(99.999%), Hydrazine hydrate, ethylene glycol, acetone, ethanol and HCl were purchased from the Shanghai Reagent Company. All the chemicals were used as obtained without further purification.

2.2. Synthesis of BTS matrix

BTS nanosheets were synthesized through a simple solution-based synthetic strategy as described in our previous report after some modifications. For the synthesis of BTS, the Bi and Te precursor solutions were separately prepared. The Te precursor solution was prepared by adding 4.8 g of NaOH, 3.48 g of TeO_2, 0.26 g of SeO_2 and 120 mL of ethylene glycol to a three-neck flask under magnetic stirring until all of them dissolved. The Bi precursor solution was prepared by dissolving 7.76 g of $Bi(NO_3)_3{\cdot}5H_2O$ in 10 mL of ethylene glycol. Then, the three-neck flask is heated to 160 °C and then the as-prepared Bi precursor solution and 2 mL Hydrazine hydrate are injected into the above solution. After reaction for another 2 h, the products were collected by filtration, successively washed several times with deionized water and absolute ethanol, and dried at 60 °C for 24 h. The as prepared BTS nanosheets pressed into pellets in a uniaxial pressure of 20 MPa, and then the pellets calcined in Ar gas at 350 °C for 1 h. The pellets were manually ground with a mortar and pestle to use as the BTS matrix of ALD.

2.3. Prepare ultrathin ZnO layer on BTS by ALD

ultrathin ZnO layer were prepared over BTS powder surface in a continuous-flow ALD reactor operated under a base pressure of ~ 1 Torr. Typically, The 5 g as-prepared BTS matrix was transferred into an ALD chamber equipped a vertical stainless rotating sample chamber. The ZnO coating layers were deposited using diethylzinc (DEZ) and H_2O as ALD precursors at 150 °C. The precursor dose and purge time were 30 s and 60 s, respectively. Ar gas served as both a carrier and a purging gas.

2.4. Characterisation

X-ray diffraction (XRD) was performed on a Bruker D8 Advance powder X-ray diffractometer; field-emission scanning electron microscopy (SEM) on a Zeiss SUPRA-55; X-ray photoelectron spectra (XPS) were acquired on Thermo Fisher ESCALAB 250 × surface analysis system equipped with a monochromatized Al anode X-ray source (X-ray photoelectron spectroscopy, XPS, $h\nu = 1486.6$ eV). The overall morphology and crystallographic information were observed with high-resolution field-emission transmission electron microscopy (FETEM; JEOL-3200FS, 300 kV). To identify the recrystallization of BTS and precipitation of Te particles at the ZnO/BTS interface, In Situ TEM were used. A focused ion beam system (FIB; JIB 4601 F, JEOL) was used to prepare the TEM samples of the sintered nanobulk composites.

2.5. Thermoelectric measurements

The dry powders pressed into pellets by hot pressed (HP) at 623 K for 1 h under vacuum with a uniaxial pressure of 60 MPa. The pellets were cylinders with 10 mm in diameter and 5 mm in height. The cuboid about 2.5 mm × 2.5 mm × 10 mm was cut to measure the thermoelectric properties using Physical properties measurement system (PPMS, Quantum Design) with thermal transport option (TTO).

3. Results and discussion

Bi_2Te_3-based thermoelectric material provide an excellent model system for systematic study on the grain boundary-related carrier/phonon transport due to its high ZT values over the temperature range of 200–400 K. [23,24] BTS nanosheets were synthesized firstly using bottom-up chemical methods that was modified from a previously reported method (Fig. S1). [5,25] As-prepared BTS nanosheets were pressed into pellets under a uniaxial pressure of 20 MPa, and then the pellets were calcined in Ar gas at 350 °C for 1 h. The pellets were manually ground with a mortar and pestle to use as the BTS matrix of ALD. The highly porous BTS substrate powder was transferred into an ALD chamber equipped with a vertical stainless rotating sample chamber for ALD coating. The ultrathin ZnO layer was deposited using diethylzinc (DEZ) and H_2O as ALD precursors at 150 °C. The as-obtained samples were hot-pressed at 623 K for 1 h under vacuum with a uniaxial pressure of 60 MPa into a φ 10 mm cylinder with 5 mm in height. The synthesis process is schematically shown in Fig. 1.

The SEM images (Fig. 2) reveal that the porous BTS powder with an average pore size about 25 nm is constructed by BTS nanoparticles with irregular shape, which ascribed to the recrystallization of BTS nanosheets during calcining process. The XRD pattern of the ALD coated samples matches well with the standard peaks of BTS (Fig. 2a). No diffraction peak of ZnO is detected because the ZnO layers are composed of only tens of atomic layers and they are amorphous, which is confirmed by the TEM and XPS results as will be discussed in following text. The 2p core level binding energies of Zn are aligned at 1044.5 eV (2p 1/2) and 1021.4 eV (2p 3/2) (Fig. 2b), and the corresponding O1s peak has a Zn-O bond (531.5 eV), which indicates the formation of ultrathin ZnO layer on the porous BTS surface. [26,27] The HRTEM images could directly confirmed the formation of ultrathin ZnO layer

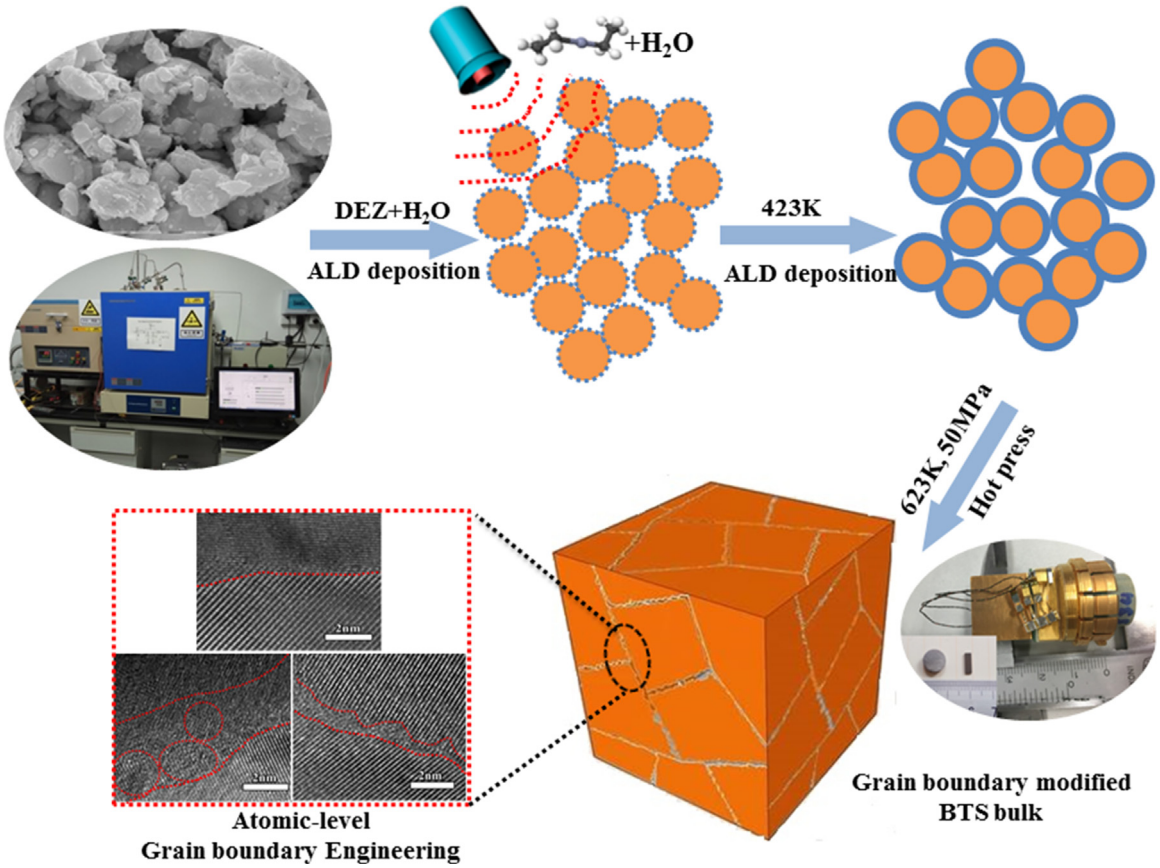

Fig. 1. A schematic of the bottom-up grain boundary engineering strategies based on atomic layer deposition (ALD) and the corresponding mechanisms contribute to high ZT.

with uniform thickness on the BTS surface. For the uncoated BTS, the surface is clean and smooth (Fig. 2f). After 20 ALD cycles, the sample surface exhibits a ~2 nm uniform and smooth coating, this is consistent with the amorphous characteristic of ALD film. HRTEM image of the BTS 60 ALD cycles shows a about 6 nm ZnO layer on the BTS surface. It is obvious that the thickness of ZnO layer followed a good linear relation with the total cycle number, suggesting that the thickness of ZnO layer can be precisely controlled by digitally varying the total ALD cycles. The growth rate of ZnO layers on the BTS surface was around 1 Å per ALD cycle, in agreement with reported data of 1.2 Å/cycle observed on most surfaces. [18,26] This result means that the thickness of ultrathin ZnO layer can be controlled at atomic level, which is significantly better than the conventional solution-based interface treatment strategy. It is noted that in all samples, the ZnO layers appears to be continuous and aggregated particles are not observed. Moreover, a well-defined interface between the ultrathin ZnO layer and BTS illustrates that the BTS particles are stable during the ALD process due to low reaction temperature. Thus, high-quality ultrathin ZnO interlayer with precise controlled thickness have been deposited on the BTS particles surface by an ALD process.

In order to deeply understand the effects of ultrathin ZnO interlayer on the carrier/phonon transport in thermoelectric material, TEM was applied to investigate the the chemical composition and microstructure of grain boundary. Considering that the hot-pressed process is crucial to the formation of grain boundary, the evolution of ZnO/BTS interface with temperature was explored by TEM experiments with in situ heating option (Fig. 3). It is clear that the BTS particle coated by a uniform and smooth ultrathin ZnO layer, consistent with the above TEM results. As temperature increases, it can be obviously seen that there are contrast changes for the BTS, indicating the recrystallization process of BTS host at high temperatures. It is found that once the temperature rose up to 573 K, the recrystallization process of BTS host is nearly complete and some small Te precipitates appear at the ZnO/BTS interface. The formation of Te precipitates could be ascribed to the high chemical activity of ultrathin ZnO layer as well as the high interfacial energy, which imposes an extra driving force of Te diffusion. The ZnO layer also act as a buffer layer to suppress the growth of Te precipitates, which results in the small size of Te precipitates. The formation of the Te nanodot at the ZnO/BTS interfaces could also be directly observed by TEM in bulk samples (Fig. 4). Typical grain boundaries were selected in order to identify their chemical compositions and structures by using HAADF (high-angle annular dark-field) imaging and EDS (energy dispersive spectrometer) imaging techniques. As revealed in STEM-HAADF image (Fig. 4a), nano-sized grains with high crystallinity possesses clean boundaries between grains. EDS imaging shows that the grain boundary is Te-rich, this agrees well with the fact that the precipitation of the Te nanodot at ZnO/BTS interface. The HAADF image (Fig. 4d) shows obvious Te nanodot with a small size of ~2 nm at the grain boundaries,which embedded in ZnO layer and connected two neighboring BTS grains. Considering the metal behavior of Te phase, the Te nanodot could serve as the efficient electron transport path between the BTS grains, which may improve the conductivity of sample. Furthermore, it should be noted that the size of Te nanodot is only about 2 nm, which may give rise to the enhanced *S* due to the quantum confinement effect. From the above analysis, it can be concluded that the ultrathin ZnO layer at BTS grain boundary could promote the precipitation of Te nanodot at the ZnO/BTS interfaces, which can be used to regulate the carrier/phonon transport property of TE sample.

The chemical composition and microstructure of grain boundary is critical to the TE performance, which can be controlled in atomic level by tuning the thickness of ZnO layer in the present sample. [28,29] To

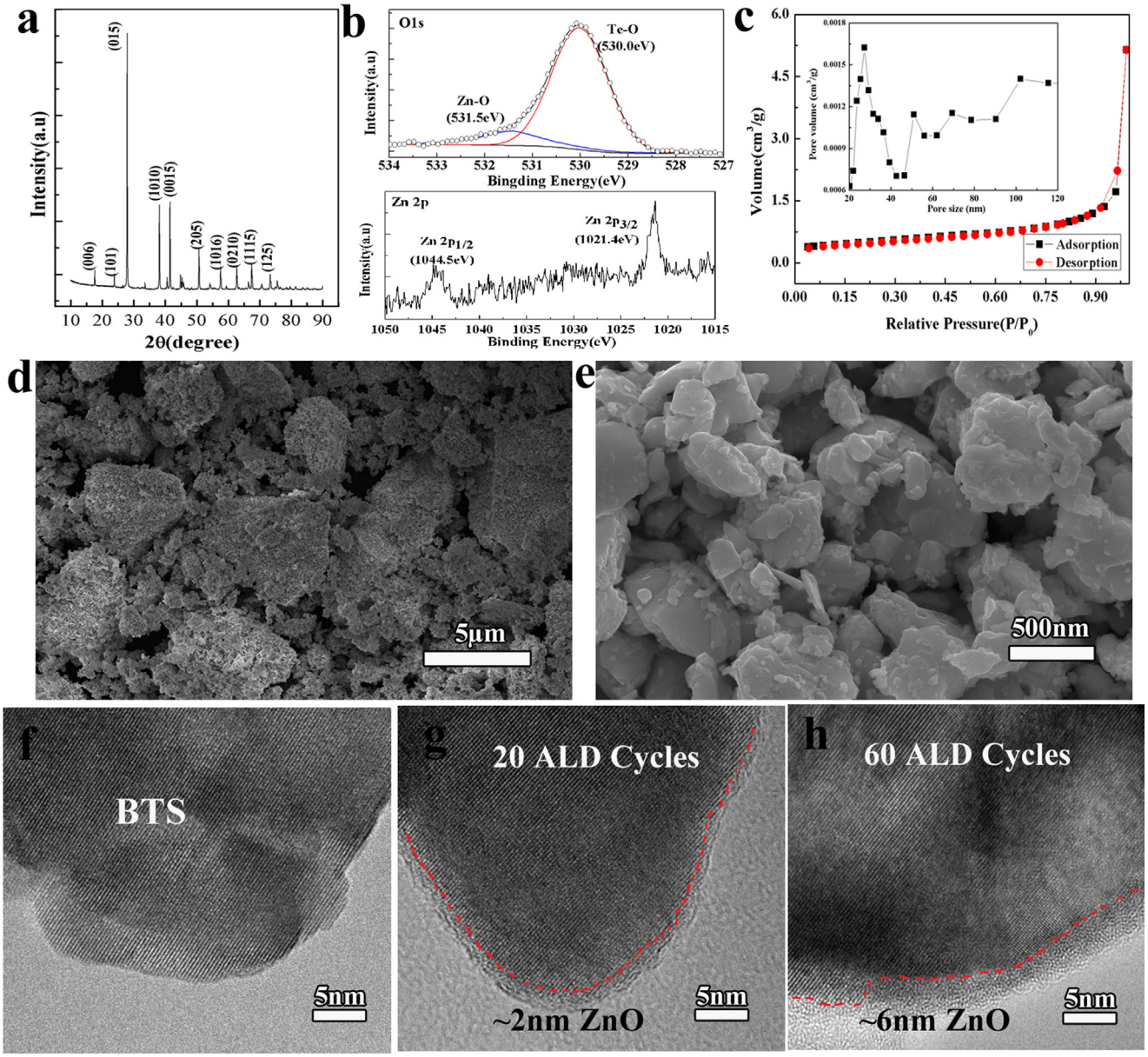

Fig. 2. (a) XRD pattern of the as-prepared BTS matrix. (b) XPS spectra for the as-prepared BTS with ultrathin ZnO interlayer. (c) Nitrogen adsorption-desorption isotherms and the corresponding pore size distribution (inset) of porous BTS powder. (d) and (e) FE-SEM image of the as-prepared porous BTS powder. (f) HRTEM image of the as-prepared BTS. (g) HRTEM image of the BTS after 20 ALD cycles. (h) HRTEM image of the BTS after 60 ALD cycles.

investigate the relationship between grain boundary microstructure and the electron/phonon transportation behavior, the detailed grain boundary structure of samples with different ALD cycles were analyzed by TEM. The pure BTS (Fig. 5**a**) show that BTS grains with an average size of about 200 nm are closely packed. Importantly, HRTEM image reveals clean boundary between grains (Fig. 5d and g), which is different from that of the sample with ultrathin ZnO layer. For the sample after 20 ALD cycles (Fig. 5b and e), the BTS grains are surrounded by 2 nm ZnO amorphous layers. It should be pointed out that the ZnO/BTS interface is sawtooth and different from the clean boundary of the pure BTS. As mentioned above, the diffusion of Te from the inside of BTS grain to the ZnO/BTS interface results in the formation of sawtooth interface. For sample after 60 ALD cycles (S60), the Te precipitation phenomenon becomes clear, which could be directly observed by TEM (Fig. 5c). The HRTEM image (Fig. 5f and k) shows obvious Te nanodot with a small size of ~2 nm at the ZnO/BTS interface. It is very interesting to observe that the Te nanodot embedded in the ZnO layer, which connecting the two BTS grains. Considering the metal behavior of Te phase, the Te nanodot could serve as the efficient electron transport path between the BTS grains. Moreover, as shown in TEM images, the average grain size also increased for the sample with ZnO layer, which is also confirmed by the XRD and SEM results (Figs. S2 and S3). The Te precipitation at the ZnO/BTS interfaces may promote the BTS grains growth in hot pressed process, which also contributes to the increased electrical conductivity. As mentioned previously, the Te precipitation only occurs at the ZnO/BTS interface, which means a proper thickness of ZnO layer is key issue to control the chemical composition and microstructure of interfaces. If the ZnO layer is too thick, the Te precipitates at interface could be divided by the ZnO layer, which suppress the electron transport between BTS grains. This argument is also consistent with the experiment results that the electrical conductivity decreased ~ 50% for the sample with thick ZnO layer (S100). Thus, precise control of the chemical composition and microstructure of grain boundary have been achieved via bottom-up grain boundary engineering strategies based on atomic layer deposition, which may provide a route to further ZT improvements.

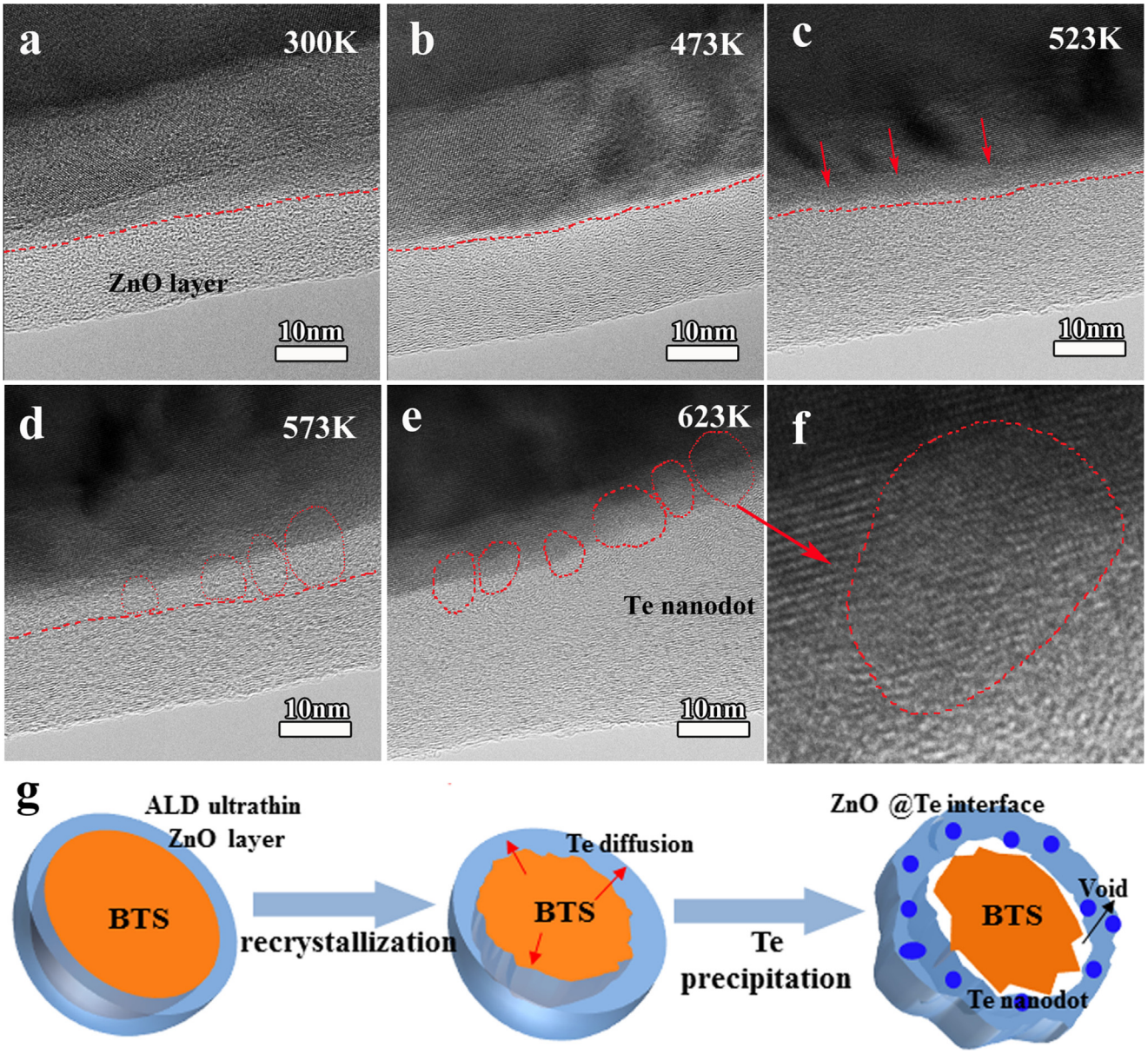

Fig. 3. In Situ TEM Observation showing the recrystallization of BTS and precipitation of Te particles at the ZnO /BTS interface in hot-pressed process. (a) 300 K, (b) 473 K, (c) 523 K, (d) 573 K, (e) 623 K,(f) HRTEM image of the Te nanodot at the ZnO/BTS interface (g) Schematic illustration of the growth mechanism of BTS/ZnO@Te in terface in the hot-pressed process.

Thus, chemical composition and microstructure of grain boundaries could be controlled by introducing ultrathin ZnO interlayer via bottom-up grain boundary engineering strategies based on ALD, which has a complex effect on the carrier/phonon transport. A combination of these interactions between interfaces microstructure and carriers could be employed to understand the electron and phonon behavior of the samples. For the pure BTS (S0), the σ (~507 S/cm at 390 K) and S (−181 μV/K) are comparable to the reported Bi_2Te_3-nanostructured bulk materials(Fig. 6). [30,31] For the grain boundary with ultrathin ZnO interlayer, the barrier at the ZnO/BTS interface is critical factor to optimize the carrier transport characteristics by energy filtering effect. Due to introducing the barriers, the σ of S10 gently decreased compared with the pure BTS (~ 20% for S10). It is noted that for S10 with very thin barriers, the tunneling carriers may contribute σ, which have negative effect on both S and $S^2\sigma$ according to the theoretical study. [13,15] This is confirmed by our results that the S10 reveals relatively low S (−185.7 μV/K) and $S^2\sigma$ (14.4 μW/cmK^2). For the S20 with wider barriers, tunneling is completely suppressed, the σ decreased due to low carrier concentration (~ $2.5*10^{19}$ cm^{-3}). We note that although the tunneling current is suppressed, the σ does not suffer significantly because the Te precipitation and sawtooth interface may produce positive effect to the σ. As mentioned above, the Te precipitations at the ZnO/BTS interfaces promote the BTS grains growth in hot pressed process, which may contributes to the high carrier mobility (~ 105 cm^2 V^{-1} s^{-1}) of S20. Furthermore, in the case of the bulk material with high σ, the barrier resistance at interface determined by the grain contact surface, which significant decreased by introducing sawtooth grain boundary. To optimize the electron transport properties, the idea potential barrier should be close to k_BT (or somewhat higher), [13] which may be fulfilled in the S20 sample. The higher $S^2\sigma$ (25.1μW/cmK^2) achieved in the S20 comes from the slightly changed σ (361 S/cm) and strongly enhanced S (−261 μV/K), which is one of the highest value reported in Bi_2Te_3-nanostructured materials (inset of Fig. 6d). [5–7,32–37] As the thickness of ZnO layer increasing, the σ (~ 100% S40 and S60) increase rapidly, which can be mainly attributed to the high carrier concentration (~ $6.2*10^{19}$ cm^{-3}) caused by Te

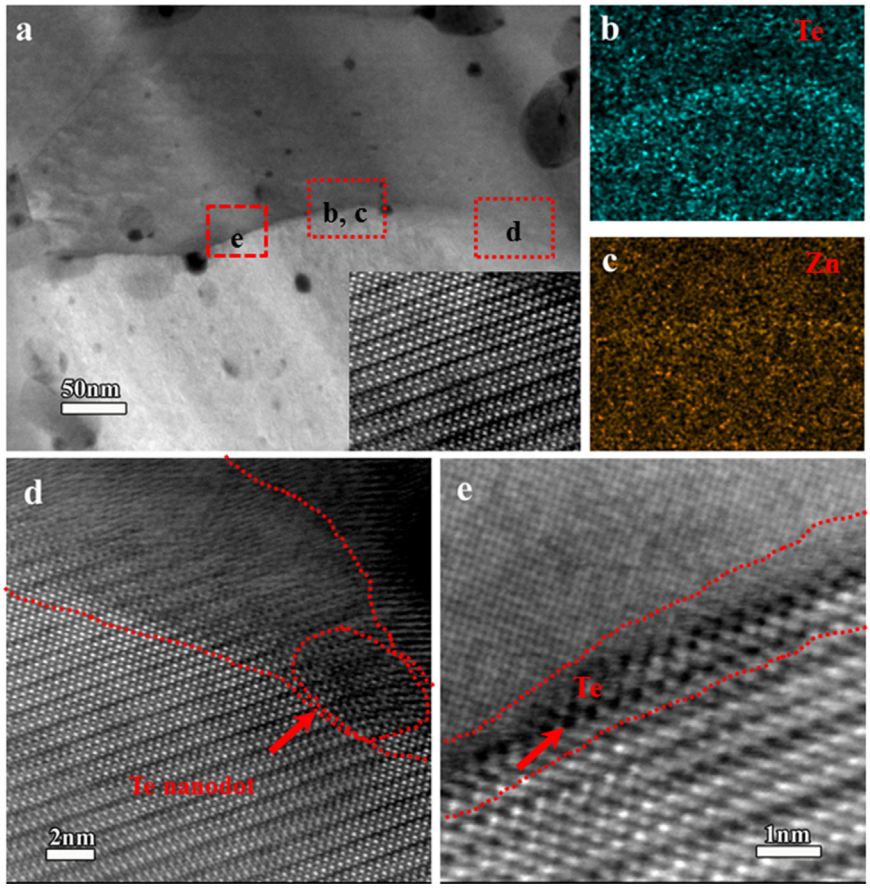

Fig. 4. (a) The low magnified STEM -HAADF image of bulk sample of S60. The EDS elemental maps of element (b) Te and (c) Zn at the selected at ultrathin ZnO layer modified grain boundary. (d) the HADDF image of the Te nanodot with a small size of ~2 nm at the grains boundaries, which connecting the two BTS grains. (e) The magnified image of the interface.

precipitation. Moreover, if the ZnO layer is too thick, the Te precipitates at interface could be separated by the ZnO layer because the Te precipitation only occurs at the ZnO/BTS interface, which suppress the electron transport between the BTS grains. This is confirmed by our result that the σ of S100 sharply decreased due to low carrier mobility and concentration.

The relation between ultrathin ZnO interlayer modified grain boundary and the carrier transport behavior could be well explained by combine the energy-filtering effects of the interface potential barrier and the Te precipitation. As theoretically predicted, the so-called "energy filtering" effect is related to the potential barriers at boundaries (related to the momentum relaxation length λ_p and the energy relaxation length λ_e) and grain size (d). [11,12] To maximize the power factor ($S^2\sigma$), the optimum potential barrier height should close to k_BT or somewhat higher, as demonstrated experimentally in many systems. [13] For a given potential barriers, the power factor can be enhanced further by grain size engineering, depending on the relationship between grain size d, the momentum relaxation length λ_p and the energy relaxation length λ_e. As we kown, the σ is not degraded much by introducing potential barriers if d is much longer than λ_p, while if d is shorter or comparable to the λ_e, then the carrier energy is not fully relaxed within the grain, so S increases. Thereby, design and control of the grain size and interface potential barrier by modifying the grain boundary to satisfy the relationship that $\lambda_p < d < \lambda_e$, S may improve without hurting σ much, which may result in a net improvement in $S^2\sigma$. [13–15] This is consistent with our results that the S is enormously improved and the σ is slightly reduced. Furthermore, in the case of the bulk material with high σ, the barrier resistance at interface determined by the grain contact surface, which may significant decreased by introducing sawtooth grain boundary due to its large grain contact surface. [11] Corresponding to S20 sample, the extraordinary structure of ZnO/BTS interface may contribute to the high σ by improving the carrier mobility (~ 104.7 cm^2V^{-1} s^{-1}). For the sample S40 and S60, the rapidly increased σ (~ 100% S40 and S60) could be contributed to the Te precipitation and the grain growth, which lead to high electrons concentration (~ 6.2*10^{19} cm^{-3}). The excess Te at the interface suggests a deficiency of Te inside the grain, which could be in the form of a Te vacancy or Bi antisite. It is known that a Te vacancy donates two electrons while a Bi antisite creates a hole, which means the precipitation of Te could contributed to the increase in electrons concentration, which agree with our results (~ 6.2*10^{19} cm^{-3}). Moreover, as mentioned previously, the increased average BTS grains size of S40 and S60 also have a positive effect on σ. Compared with the pure BTS (S0), the carrier mobility (~ 80 cm^2 V^{-1} s^{-1}) decreased, which may be the result of compound of interface barrier and structure. For the BTS/ZnO@Te interface that ~ 2 nm Te nanodot embedded in the amorphous ZnO layers, the Te nanodot could serve as the efficient electron transport path between the BTS grains due to its metal behavior, which may have a positive effect on carrier mobility. However, for the sample S40 and S60, the effective grain contact surface (equal to the electron transport path between the BTS grains) is much less than that of the pure BTS due to the small size of Te nanodot. This may have a negative effect to the carrier mobility as mentioned above. The thick ZnO layer at grain boundary could suppress the electron transport between BTS grains, which confirmed by the experiment results that the electrons mobility and concentration decreased the sample S100 with thick ZnO layer. All of the above discussion is consistent with the RT Hall measurements results (Table S1).

To clarify the electronic transport behavior in as-prepared samples, the S as a function of carrier concentration (n) is plotted. For a highly degenerate semiconductor, the S can be expressed as follows,

$$S = \frac{8\pi^2 k_B^2}{3eh^2}\left(\frac{\pi}{3n}\right)^{\frac{2}{3}} m_d^* T$$

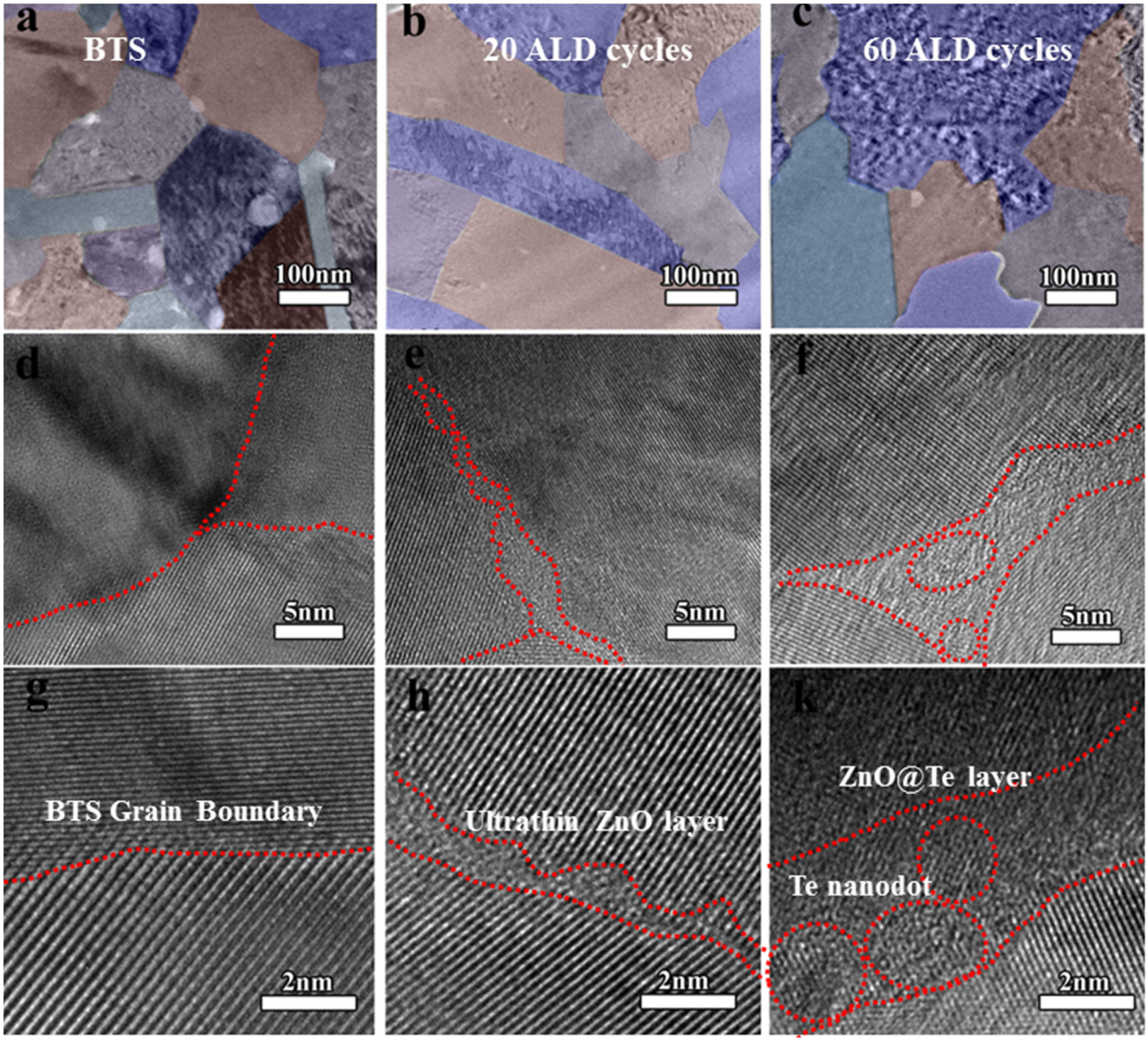

Fig. 5. TEM characterizations of the ultrathin ZnO layer modified BTS grain boundary with different ALD cycles. (a) Low magnification TEM image, (d) (g) HRTEM images at the grain boundaries of S0. (b) Low magnification TEM image, (e) (h) HRTEM images at the ZnO/BTS interface of S20. (c) Low magnification TEM image, (f) (k) HRTEM images at the BTS/ZnO@Te interface of S60.

where m_d* is the density of states (DOS) effective mass, and k_B, e, and h are the Boltzmann constant, elementary charge, and the Planck constant, respectively. By utilizing the S and n values at room temperature, the m_d* was determined and compared with literature data in in Fig. 6c. [5–7,35,38] The m_d* values of BTS (~ 0.8 m_0) is almost the same to the previously reported n-type BT-based materials. However, for the S20, the m_d* increases to ~ 1 m_0 due to the optimized potential barrier and interface microstructure, which could be responsible for large |S|. Larger m* value of S40 (~ 1.2 m_0) and S60 (~ 1.2 m_0) can be mainly attributed to high carrier concentration, which shows a weaker effect on S. [24] Thus, as previously mentioned, chemical composition and microstructure of grain boundaries related optimization regulation of the electron transport properties is the key-issue to enhance TE performance of the present sample.

As is well known, the total thermal conductivity (κ_{tot}) of TE semiconductors could be expressed as $\kappa_{tot} = \kappa_e + \kappa_{latt} + \kappa_{bi,}$ in which κ_e is thermal conductivity of electronic contribution, κ_{latt} is the lattice thermal conductivity, and κ_{bi} is the bipolar thermal conductivity. [39,40] The κ_e was estimated according to the Wiedemann-Franz law $\kappa_e = L\sigma T$, where the Lorenz number L was calculated using an approximation equation L= 1.5 +exp (-|S|/116). Fig. 7 shows the thermal conductivity of the samples. Three distinct regions are apparent, depending on the thickness of ZnO layer, corresponding to the electron transport behavior. The ultrathin ZnO layer (1–2 nm) at the interface only slightly affects the phonon transport, where the κ_{latt} shows no obvious change compared with the pure BTS sample. As we discussed previously, the precipitation of Te nanodot and increasing of average BTS grains size contribute to the high κ_{latt} for the S40 and S60. For S100, the ZnO layer with a thickness of about 10 nm could effective enhance the phonon scattering, resulting in the sharp decline of $\kappa_{latt.}$ It should be noted that at high temperature region (T > 350 K), the κ_{tot} -κ_e of all samples with ultrathin ZnO layer became smaller than that of pristine BTS, which can be ascribed to the suppression of κ_{bi} by ZnO/BTS interfaces. It is well known that the phonon scattering by Umklapp mechanism leads to a T^{-1} temperature dependence of κ_{latt} as the T above Debye temperature (the Debye temperature of Bi_2Te_3-based

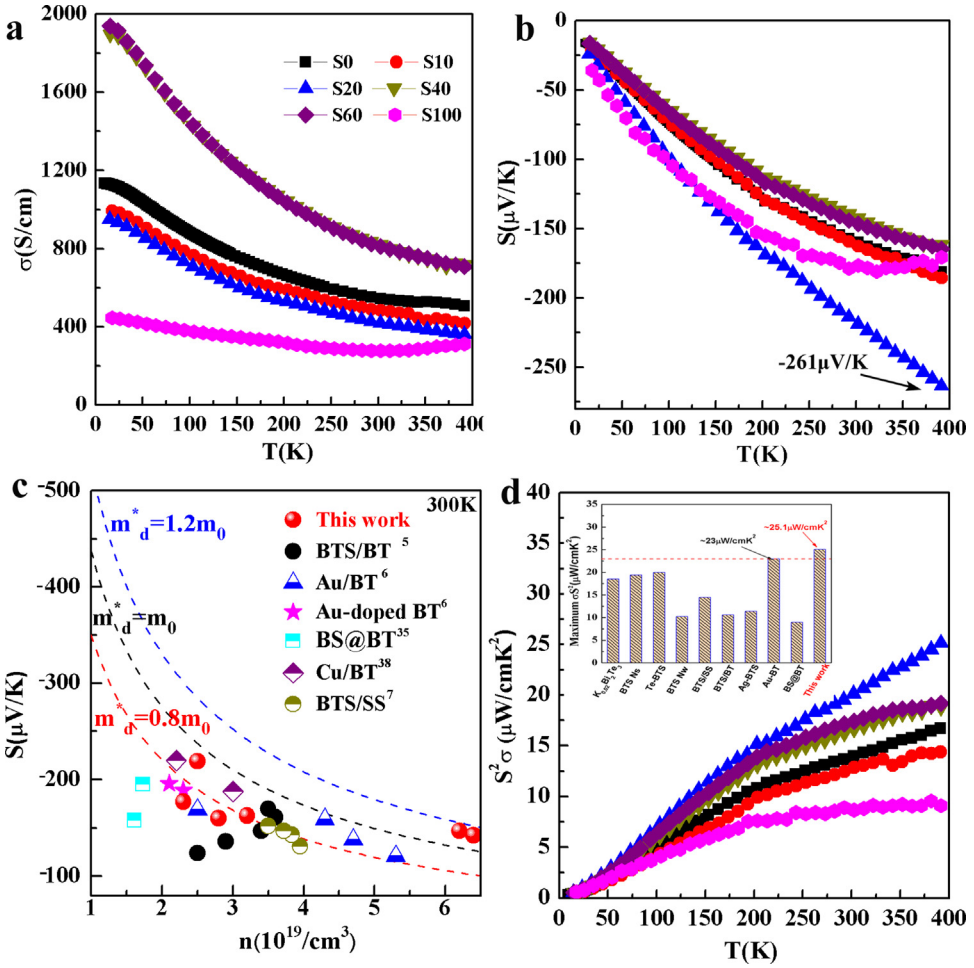

Fig. 6. The electrical transport properties of the ultrathin ZnO layer modified sample with different ALD cycles. (a) Electrical conductivity (σ), (b) Seebeck coefficient (S), (c) Seebeck coefficient (S) as a function of carrier concentration (n). (d) Power factor ($S^2\sigma$), the inset is the comparison of the maximum $S^2\sigma$ of this work with provious reported Bi_2Te_3-based nanomaterials. ($K_{0.06}Bi_2Te_3$ Nanotubes ($K_{0.06}Bi_2Te_3$), exfoliated $Bi_2Te_{2.7}Se_{0.3}$ nanosheets (BTS NS), Te-$Bi_2Te_{2.7}Se_{.3}$ nanosheets (Te-BTS), $Bi_2Te_{2.7}Se_{0.3}$ nanowires (BTS NW), $Bi_2Te_{2.7}Se_{0.3}/SnS_2$ nanocomposite (BTS/SS), $Bi_2Te_{2.7}S_{0.3}/Bi_2Te_3$ hetero-nanosheet (BTS/BT), silver nanoparticles-dispersed Bi_2Te_3 composites (Ag-BT), Au nanodot-included Bi_2Te_3 nanotube composites (Au-BT), Bi_2Se_3 @ Bi_2Te_3 heterostructured nanoplates(BS@BT)).

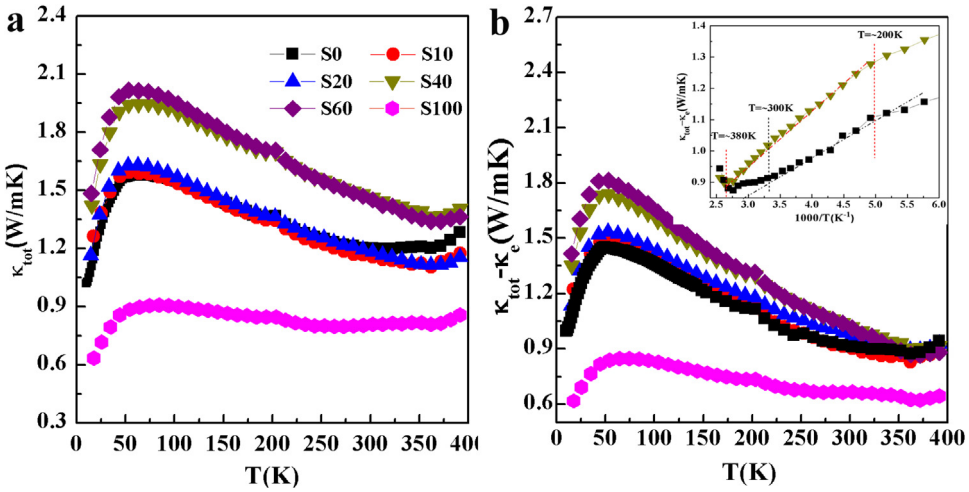

Fig. 7. (a) Temperature dependence of κ_{tot} for the ultrathin ZnO layer modified sample with different ALD cycles. (b) lattice thermal conductivity ($\kappa_{latt.}$) calculated by subtracting the electronic thermal conductivity (κ_e) from the total thermal conductivity (inset is the ($\kappa_{tot} - \kappa_e$) vs 1000/T).

materials is around 145 K [41]), while bipolar effect contributes to the increase of thermal conductivity at higher temperature (> 300 K). [36] The κ_{tot} -κ_e of pristine BTS is a combination of Umklapp process (T^{-1} dependence, 200K-300K) and bipolar effects, and the bipolar effects start to overcome the Umklapp process when temperature increases above 300 K. However, the samples with ultrathin ZnO interlayer exhibit the linear behavior with T^{-1} dependence (from Umklapp process) from 200 to 370 K, indicating the suppression of κ_{bi}. The κ_{bi} originates from the bipolar thermodiffusion process in the material and is approximately given near the intrinsic regime by

$$\kappa_{bi} \propto \exp\left(-\frac{E_g}{2k_B T}\right)$$

where *Eg* is the band gap, and k_B is the Boltzmann constant. [11] For the sample with optimized incorporating heterostructure barriers, the minority carriers are prevented from participating in conduction and

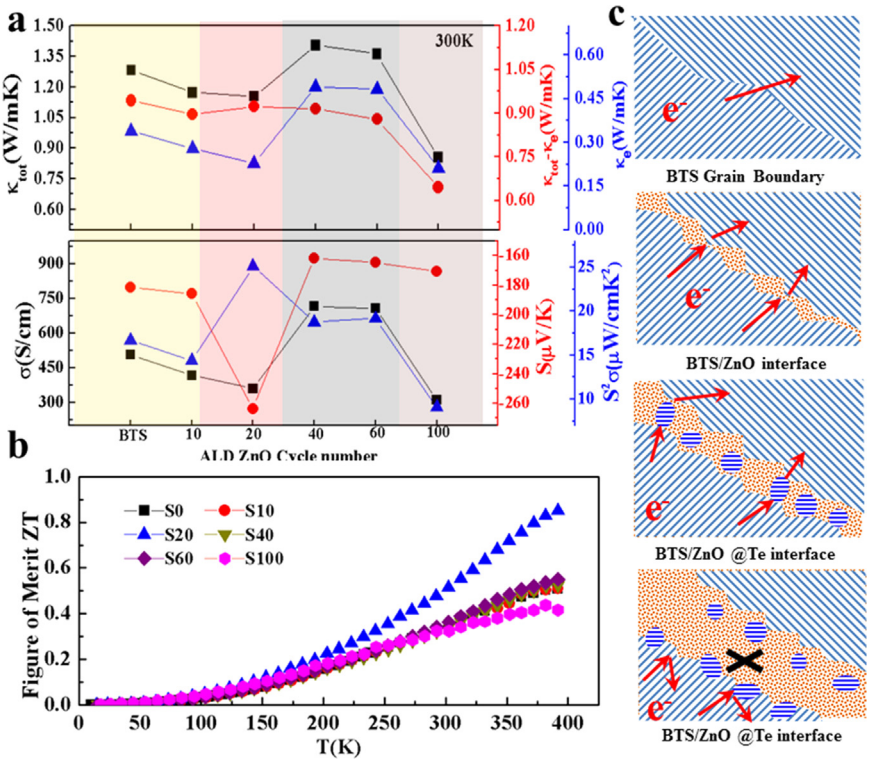

Fig. 8. (a) Thickness of ALD ZnO layer (corresponding to the ALD cycle namber) dependent the thermal and electronic transport properties at 300 K. (b)Thermoelectric figure of merit ZT of the the ultrathin ZnO layer modified sample. (c) The sketch of electronic transmission path at different ultrathin ZnO layer modified BTS grain boundary.

the majority carriers are not much affected, then the significant suppression of κ_{bi} could be achieved. For the as-prepared sample, the increase of carrier density, the existence of the energy barrier at the ZnO/BTS interface, and nanosized grain and Te nanodot at grain boundaries can all contribute to the suppression of bipolar effect.

Due to the optimization regulation of the electron and phonon transport properties by the ZnO/BTS interface, the figure of merit ZT is improved significantly, as shown in Fig. 8**b**. The highest ZT reaches 0.85 at 390 K for S20 due to its ultrahigh $S^2\sigma$ and relatively low κ_{tot}, which is ~ 80% higher than that of pristine BTS. Compared with other n-type BT-based nanostructures TE materials, it is an excellent and highly competitive value in the near room temperature range, [5–7,36] which could be further enhanced by optimizing the energy barriers of interface and adopting high performance pristine TE materials. As a whole, the simultaneous optimization of electrical and thermal transport properties via the ALD based atomic scale grain boundary modification strategy has achieved, as schematically illustrated in Fig. 8c. Furthermore, the further prospect of this study is to modify the interface potential barrier by depositing other semiconductor layer (such as SnO_2, TiO_2) on the matrix and further extending the ALD based atomic scale grain boundary modification strategy to other thermoelectric materials system. This study creates an initial attempt to modify the grain boundary of bulk thermoelectric materials in atomic scale by ALD process, which provides the insights for the structural design and synthesis of broadly functional hybrid thermoelectric material system.

4. Conclusions

In summary, we demonstrate that bottom-up grain boundary engineering strategies based on atomic layer deposition could be introduced to design and control grain boundary in atomic scale, which could be extended to other thermoelectric materials system simply. As an initial attempt, ultrathin ZnO layer with precise controlled thickness was introduced at the BTS grain boundary to investigate the chemical composition and structure of grain boundary related electron/phonon transportation behavior. It is found that the atom-level control over the chemical composition and structure of grain boundary could be achevied by adjusting ZnO layer thickness due to the promoting effect of ZnO layer to the precipitation of Te nanodot at ZnO/BTS interface. By optimizing the potential barrier and grain size by grain boundary engineering, the strongly enhanced S and high $S^2\sigma$ because of the energy filtering effect, which is about 2 times higher than that of the pure BTS sample. Moreover, it is found that the designed ZnO/BTS interface could suppress the bipolar thermal conductivity at high temperature region. The bottom-up grain boundary engineering strategies based on atomic layer deposition provides a novel approach to optimize the dimension and composition of grain boundary. This effective approach can be adopted to other thermoelectric material system simply, which will contribute to the development of high performance thermoelectric material of great significance.

Acknowledgment

The work was financially supported by National Materials Genome Project (2016YFB0700600), Shenzhen Science and Technology Research Grant (No. JCYJ20150629144612861, JCYJ20150827155136104), China Postdoctoral Science Foundation funded project (No. 2016M600862), Shenzhen Key Science and Technology Plan (No. JSGG20141118144410953), Guangdong applied technology research special project (No. 2015B090927003), the National Natural Science Foundation of China (Grant No. 51602143).

Supporting information

The details on syntheses, powder X-ray diffraction, scanning electron microscopy, and thermoelectric measurements supplied in Supporting Information.

Appendix A. Supporting information

Supplementary data associated with this article can be found in the online version at http://dx.doi.org/10.1016/j.nanoen.2018.04.047.

References

[1] J. He, T.M. Tritt, Science 357 (6358) (2017) 1369.
[2] G.J. Snyder, E.S. Toberer, Nat. Mater. 7 (2008) 105–114.
[3] M.G. Kanatzidis, MRS Bull. 40 (2015) 687.
[4] M.M. González, O.C. Calero, P.D. Chao, Renew. Sustain. Energy Rev. 24 (2013) 288–305.
[5] S. Li, C. Xin, X. Liu, Y. Feng, Y. Liu, J. Zheng, F. Liu, Q. Huang, Y. Qiu, J. He, J. Luo, F. Pan, Nano Energy 30 (2016) 780–789.
[6] E. Lee, J. Ko, J.-Y. Kim, W.-S. Seo, S.-M. Choi, K.H. Lee, W. Shime, W. Lee, J. Mater. Chem. C 4 (2016) 1313–1319.
[7] S. Li, X. Liu, Y. Liu, F. Liu, J. Luo, F. Pan, Nano Energy 39 (2017) 297–305.
[8] W.G. Zeier, A. Zevalkink, Z.M. Gibbs, G. Hautier, M.G. Kanatzidis, G.J. Snyder, Angew. Chem. Int. Ed. 55 (2016) 2–18.
[9] J.R. Sootsman, D.Y. Chung, M.G. Kanatzidis, Angew. Chem. Int. Ed. 48 (2009) 8616–8639.
[10] B. Moyzhes, V. Nemchinsky, Appl. Phys. Lett. 73 (1998) 1895.
[11] R. Kim, M.S. Lundstrom, J. Appl. Phys. 111 (2012) 024508.
[12] J.-H. Bahk, A. Shakouri, Appl. Phys. Lett. 105 (2014) 052106.
[13] R. Kim, M.S. Lundstrom, J. Appl. Phys. 110 (2011) 034511.
[14] S. Sadasivam, U.V. Waghmare, T.S. Fisher, J. Appl. Phys. 117 (2015) 134502.
[15] M. Thesberg, H. Kosina, N. Neophytou, J. Appl. Phys. 120 (2016) 234302.
[16] Y. Ouyang, Y. Xie, Z. Zhang, Q. Peng, Y. Chen, J. Appl. Phys. 120 (2016) 235109.
[17] L. Hu, H. Wu, T. Zhu, C. Fu, J. He, P. Ying, X. Zhao, Adv. Energy Mater. 5 (2015) 1500411.
[18] L. Ma, R.B. Nuwayhid, T. Wu, Y. Lei, K. Amine, J. Lu, Adv. Mater. Interfaces (2016) 1600564.
[19] X. Zhang, I. Belharouak, L. Li, Y. Lei, J.W. Elam, A. Nie, X. Chen, R.S. Yassar, R.L. Axelbaum, Adv. Energy Mater. 3 (2013) 1299–1307.
[20] L.E. Black, A. Cavalli, M.A. Verheijen, J.E.M. Haverkort, E.P.A.M. Bakkers, W.M.M. Kessels, Nano Lett. 17 (10) (2017) 6287–6294.
[21] Q. Lin, Y. Su, M. Zhang, X. Yang, S. Yuan, J. Hu, Y. Lin, J. Liang, F. Pan, Chem. Commun. 52 (2016) 10708.
[22] T. Tynell, M. Karppinen, Semicond. Sci. Technol. 29 (2014) 043001.
[23] S. Singh, H. Mun, S. Lee, S.W. Kim, S. Baik, Adv. Mater. 29 (2017) 1701988.
[24] Y. Yu, D.-S. He, S. Zhang, O.C. Mirédinc, T. Schwarz, A. Stoffersd, X.-Y. Wang, S. Zheng, B. Zhu, C. Scheud, D. Wu, J.-Q. He, M. Wuttig, Z. –Y. Huang, F.-Q. Zu, Nano Energy 37 (2017) 203–213.
[25] D.L. Medlin, G.J. Snyder, Curr. Opin. Colloid Interface Sci. 14 (2009) 226–235.
[26] J.-Z. Kong, H.-F. Zhai, X. Qian, M. Wang, Q. –Z. Wang, A.-D. Li, H. Li, F. Zhou, J. Alloy. Compd. 694 (2017) 848–856.
[27] B. Zhu, N. Liu, M. McDowell, Y. Jin, Y. Cui, J. Zhu, Nano Energy 13 (2015) 620.
[28] G. Tan, L.-D. Zhao, M.G. Kanatzidis, Chem. Rev. 116 (19) (2016) 12123–12149.
[29] J. Mao, Y. Wang, Z. Liu, B. Ge, Z. Ren, Nano Energy 32 (2017) 174–179.
[30] S. Li, T. Fan, X. Liu, F. Liu, H. Meng, Y. Liu, F. Pan, ACS Appl. Mater. Interfaces 9 (2017) 3677–3685.
[31] C. Zhou, C. Dunc, K. Wang, X. Zhang, Z. Shi, G. Liu, C.A. Hewitt, G. Qiao, D.L. Carroll, Nano Energy 30 (2016) 709–716.
[32] K. Park, K. Ahn, J. Cha, S. Lee, S.I. Chae, S.-P. Cho, S. Ryee, J. Im, J. Lee, S.-D. Park, M.J. Han, I. Chung, T. Hyeon, J. Am. Chem. Soc. 138 (43) (2016) 14458–14468.
[33] M. Hong, T.C. Chasapis, Z.-G. Chen, L. Yang, M.G. Kanatzidis, G.J. Snyder, J. Zou, ACS Nano 10 (4) (2016) 4719–4727.
[34] Q. Zhang, X. Ai, L. Wang, Y. Chang, W. Luo, W. Jiang, L. Chen, Adv. Funct. Mater. 25 (2015) 966–976.
[35] Y. Min, G. Park, B. Kim, A. Giri, J. Zeng, J.W. Roh, S. Il Kim, K.H. Lee, U. Jeong, ACS Nano 9 (7) (2015) 6843–6853.
[36] C. Zhang, M.D.L. Mata, Z. Li, F.J. Belarre, J. Arbiol, K.A. Khor, D. Poletti, B. Zhu, Q. Yan, Q. Xiong, Nano Energy 30 (2016) 630–638.
[37] G. Zhang, B. Kirk, L.A. Jauregui, H. Yang, X. Xu, Y.P. Chen, Yue Wu, Nano Lett. 12 (2012) 56–60.
[38] M.-K. Han, K. Ahn, H.J. Kim, J.-S. Rhyee, S.-J. Kim, J. Mater. Chem. 21 (2011) 11365–11370.
[39] B. Xu, M.T. Agne, T. Feng, T.C. Chasapis, X. Ruan, Y. Zhou, H. Zheng, J.-H. Bahk, M.G. Kanatzidis, G.J. Snyder, Yue Wu, Adv. Mater. 29 (10) (2017) 1605140–1605148.
[40] D. Ding, D. Wang, M. Zhao, J. Lv, H. Jiang, C. Lu, Z. Tang, Adv. Mater. 29 (2017) 1603444.
[41] P. Puneet, R. Podila, M. Karakaya, S. Zhu, J. He, T.M. Tritt, M.S. Dresselhaus, A.M. Rao, Sci. Rep. 3 (2013) 3212.

Dr. Shuankui Li received his Ph.D. degree in Condensed Matter Physics in 2014 from Lanzhou University, China. He is currently a post-doctoral fellow at School of Advanced Materials, Peking University, Shenzhen Graduate School with a research focus on design and preparation high performance nanostructured thermoelectrics materials.

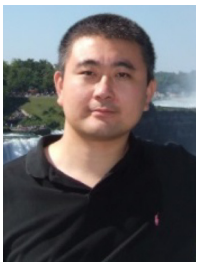

Dr Yidong Liu is currently distinguished researcher in School of Advanced Materials, Peking University Shenzhen Graduate School. He received his Ph.D. in Chemistry from the Graduate Center/ CUNY in 2006. After his Ph.D., he moved to Columbia University as an associate research scientist. His research concentrates in high performance materials, composite and devices.

Fu-Sheng Liu received his Ph.D. in condensed matter physics in 2005 from Institute of Physics, Chinese Academy of Sciences (CAS), China. From 2005 to now, he joined in Shenzhen University as a full professor. His current research interests include crystal structure, metallic functional materials, thermoelectric materials and their related properties. He has authored and co-authored more than 100 refereed journal publications.

Professor Jun Luo received his Ph.D. in Condensed Matter Physics from the Institute of Physics, Chinese Academy of Science, in 2005. Then, he was awarded an Alexander von Humboldt Research Fellowship to visit Free University of Berlin. He went back to Institute of Physics, Chinese Academy of Science, in 2007, and worked there for 7 years. In October of 2013, he moved to Shanghai University and continued his work on thermoelectric materials.

Prof. Feng Pan, National 1000-plan Professor, Founding Dean of School of Advanced Materials , Peking University Shenzhen Graduate School, Director of National Center of Electric Vehicle Power Battery and Materials for International Research, got B.S. from Dept. Chemistry, Peking University in1985 and Ph.D. from Dept. of P&A Chemistry , University of Strathclyde, Glasgow, UK, with "Patrick D. Ritchie Prize" for the best Ph.D. in 1994. With more than a decade experience in large international incorporations, Prof. Pan has been engaged in fundamental research and product development of novel optoelectronic and energy storage materials and devices. As Chief Scientist, Prof. Pan led 8 entities in Shenzhen to win the 150 million RMB grant for the national new energy vehicles (power battery) innovation project from 2013 to end of 2015. As Chief Scientist, Prof. Pan led 12 entities to win National Key project of Material Genomic Engineering for Solid State Li-ion Battery in China in 2016.